Natural Embedding of the Stokes Parameters of Polarimetric Synthetic Aperture Radar Images in a Gate-Based Quantum Computer

Soronzonbold Otgonbaatar and Mihai Datcu, *Fellow, IEEE*

***Abstract*— Quantum algorithms are designed to process quantum data (quantum bits) in a gate-based quantum computer. They are proven rigorously that they reveal quantum advantages over conventional algorithms when their inputs are certain quantum data or some classical data mapped to quantum data. However, in a practical domain, data are classical in nature, and they are very big in dimension, size, and so on. Hence, there is a challenge to map (embed) classical data to quantum data, and even no quantum advantages of quantum algorithms are demonstrated over conventional ones when one processes the mapped classical data in a gate-based quantum computer. For the practical domain of earth observation (EO), due to the different sensors on remote-sensing platforms, we can map directly some types of EO data to quantum data. In particular, we have polarimetric synthetic aperture radar (PolSAR) images characterized by polarized beams. A polarized state of the polarized beam and a quantum bit are the Doppelganger of a physical state. We map them to each other, and we name this direct mapping a *natural embedding*, otherwise an *artificial embedding*. Furthermore, we process our *naturally embedded* data in a gate-based quantum computer by using a quantum algorithm regardless of its quantum advantages over conventional techniques; namely, we use the QML network as a quantum algorithm to prove that we *naturally embedded* our data in input qubits of a gate-based quantum computer. Therefore, we employed and directly processed PolSAR images in a QML network. Furthermore, we designed and provided a QML network with an additional layer of a neural network, namely, a hybrid quantum-classical network, and demonstrate how to program (via optimization and backpropagation) this hybrid quantum-classical network when employing and processing PolSAR images. In this work, we used a gate-based quantum computer offered by an IBM Quantum and a classical simulator for a gate-based quantum computer. Our contribution is that we provided very specific EO data with a *natural embedding* feature, the Doppelganger of quantum bits, and processed them in a hybrid quantum-classical network. More importantly, in the future, these PolSAR data can be processed by future quantum algorithms and future quantum computing platforms to obtain (or demonstrate) some quantum advantages over conventional techniques for EO problems.**

***Index Terms*— Natural embedding, parameterized quantum circuit, polarimetric synthetic aperture radar (PolSAR), quantum machine learning (QML).**

I. Introduction

RECENT breakthroughs in building a gate-based quantum computer with very few quantum bits (qubits) [1] and in applying machine learning (ML) techniques to any annotated datasets led to a quantum algorithm called quantum ML (QML) being considered as a promising disruptive technique for a particular class of supervised learning methods [2]–[5], [6]. A quantum algorithm is an algorithm being processed in quantum computers, and a QML network is the network of *parameterized quantum gates* in a gate-based quantum computer. There is growing interest to apply a QML network to classical data [7], [8]. However, the gate-based quantum computer itself is posing several new challenges, for instance, how to map classical data to qubits (quantum data) depending on the limited number of its input qubits, or how to use the specificity of the "qubits" to obtain quantum advantages over nonquantum computing techniques, while ubiquitous data in practical domains are of classical nature. In particular, the input data play an important role in a quantum algorithm to obtain quantum advantages, and for example, in scientific studies [9], [10], their authors implied that QML networks achieve quantum advantages over a conventional technique only if classical data are *naturally* embedded in their input qubits, or their input data are quantum data.

Some studies proposed to embed classical data (e.g., RGB images) in quantum data by exploiting a conventional deep neural network (DNN) for its dimensionality reduction [11], [12]. Such an embedding procedure of classical data is named an *artificial embedding*, otherwise a *natural embedding*. Moreover, their QML network classifies *artificially* embedded data in qubits with no physical information even if the qubits carry physical information.

In this article, we introduce and provide a classical remotely sensed dataset with a *natural embedding* feature; in particular, we use polarimetric synthetic aperture radar (PolSAR) images of earth observation (EO) [13]–[15]. Then, we use the QML network as a quantum algorithm for processing our PolSAR images to prove that we *naturally* embedded our PolSAR data in qubits. The PolSAR images are obtained by using a PolSAR imaging technique. The PolSAR technique measures a scattering matrix S related to the incident and reflected Jones vector on the ground scene. The scattering matrix S preserves the physical scattering properties of the polarization-changing targets (e.g., *water*, *urban area*, and *vegetation*) [see Fig. 1(a)] [16]–[18].

More importantly, the PolSAR image can be represented by a number of Stokes parameters by assuming incident Jones vectors [19]. In this article, we represent the targets in a given PolSAR image by five Stokes parameters when assuming five

Manuscript received July 15, 2021; accepted August 31, 2021. *(Corresponding authors: Soronzonbold Otgonbaatar; Mihai Datcu.)*

Soronzonbold Otgonbaatar is with German Aerospace Center (DLR), 82234 Weßling, Germany (e-mail: soronzonbold.otgonbaatar@dlr.de).

Mihai Datcu is with German Aerospace Center (DLR), 82234 Weßling, Germany, and also with Politehnica University of Bucharest (UPB), 060042 Bucharest, Romania (e-mail: mihai.datcu@dlr.de).

Digital Object Identifier 10.1109/TGRS.2021.3110056

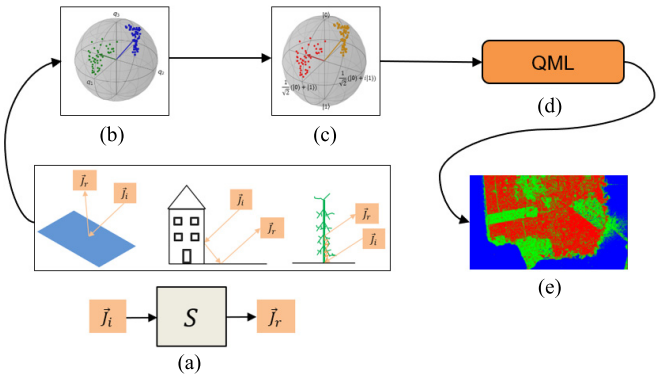

Fig. 1. This article in a pictorial representation. (a) Targets in a PolSAR image have different physical scattering properties for an incident Jones vector (a free variable). Given the incident Jones vector and given any polarization-changing target of a PolSAR image, we obtain a reflected Jones vector; $\vec{J}_i \xrightarrow{S} \vec{J}_r$, where S stands for the polarization-changing target/pixel of a given PolSAR image. (b) Stokes parameters. (c) Qubits. (d) QML network. (e) Outputs of the QML network that yields information about the polarization-changing targets in a PolSAR image.

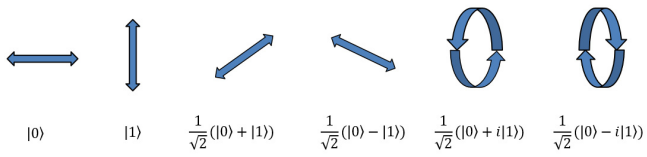

Fig. 2. Doppelganger role of Jones vectors and qubits. (Top) Jones vectors. (Left to Right) Horizontal, vertical, diagonal-up and -down, and left- and right-circular polarized states. (Bottom) Corresponding qubits.

different incident Jones vectors. Furthermore, the Jones vector is the Doppelganger of qubits (see Fig. 2), and the Stokes parameters then have one-to-one correspondences with the qubits; a qubit (or a two-state qubit) $|\psi\rangle \in \mathbb{C}^2$, $|\psi\rangle \in \{|0\rangle, |1\rangle\}$ is the quantum version of classical bits, and they can exist in superposition. This one-to-one correspondence property allows us to employ and process the PolSAR images as the input data of a QML network. Thus, we first *naturally* embed the Stokes parameters in qubits [see Fig. 1(b) and (c)]. Second, we demonstrate how to program (by optimization and back-propagation) the QML network and a hybrid quantum-classical network when employing and processing PolSAR images as its input data [see Fig. 1(d) and (e)]. The hybrid quantum-classical network is a learning network where the output of the QML network is connected to a layer of neurons. As real-world data, we use a C-band PolSAR image of *San Francisco*, USA, obtained from Radarsat-2, and L-band PolSAR image of *Oberpfaffenhofen*, Germany, taken by ESAR-L airborne.

This work is structured as follows. In Section II, we first provide some background on the Stokes parameters of our PolSAR images, and second, we derive the Stokes parameters of PolSAR images *San Francisco* and *Oberpfaffenhofen* in Section III and then propose a QML network as a hybrid quantum-classical network (see Section IV). Finally, we demonstrate how to program a hybrid quantum-classical network when applying synthetic quantum data as its input, and we validate that the Stokes parameters convey information about polarization-changing targets in PolSAR images by training them on a hybrid quantum-classical network (see Sections V and VI). Finally, we draw a conclusion in Section VII.

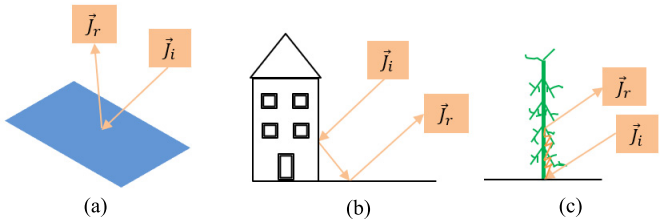

Fig. 3. Physical scattering properties of polarization-changing targets. (a) Single-bounced beam on *water surface*. (b) Double-bounced beam on *corners of some targets*. (c) Volume-scattered beam in *trees* and a medium.

II. Stokes Parameters of PolSAR Images Derived by PolSAR Techniques

A. Introduction to the PolSAR Technique

A PolSAR system measures a 2×2 scattering matrix S of a beam characterizing targets in a ground scene at a given incident angle. The scattering matrix of a PolSAR image can be expressed by

$$S = \begin{pmatrix} s_{HH} & s_{HV} \\ s_{VH} & s_{VV} \end{pmatrix} \tag{1}$$

where each element of S is a complex-valued number; the first index of an element $s_{ij}, i, j \in \{H, V\}$ represents the polarization state of the incident polarized beam, and the second index represents the polarization state of the reflected polarized beam on targets [16], [17]. This scattering matrix preserves information on polarization-changing ground targets (see Figs. 1 and 3). The off-diagonal elements of S are equal $s_{VH} = s_{HV}$ when PolSAR images (e.g., *San Francisco* and *Oberpfaffenhofen*) are fully polarized PolSAR images obtained by a monostatic radar.

Furthermore, the ground targets imagined in a PolSAR image have disparate physical scattering properties, e.g., geometrical structures, scattering each incident polarized beam from a PolSAR system differently. For example, an incident polarized beam on a rough surface (water) has the scattering properties of a single-bounced beam, the incident polarized beam on some corners of buildings has the scattering properties of a double-bounced beam, and the incident polarized beam on trees has the scattering properties of a volume-scattered beam (see Fig. 3). These different scattering properties of any targets are represented by a so-called Pauli vector. The Pauli vector can be written as

$$\begin{aligned} \mathbf{k} &= \frac{1}{\sqrt{2}}(s_{HH} + s_{VV} \quad s_{HH} - s_{VV} \quad 2s_{HV})^{\mathrm{T}} \\ &= \frac{1}{\sqrt{2}}(k_1 \quad k_2 \quad k_3)^{\mathrm{T}} \end{aligned} \tag{2}$$

where subscript T represents transposition, and k_1, k_2, and k_3 represent a single-bounced beam, a double-bounced beam, and a volume-scattered beam, respectively [16], [17], [20].

B. Derivation of Stokes Parameters

An incident/reflected beam on the ground scene can be expressed by

$$\vec{E} = \vec{E}_0 \exp i\phi \tag{3}$$

where ϕ is a phase, and $\vec{E}_0$ is a complex amplitude vector of an incident/reflected beam. A complex amplitude vector can be expressed in a polarization basis $\{H, V\}$ by

$$\vec{E}_0 = E_{H0}\hat{H} + E_{V0}\hat{V}. \tag{4}$$

This complex amplitude vector can be rewritten as

$$\vec{J} = \begin{pmatrix} E_{H0} \\ E_{V0} \end{pmatrix} = \begin{pmatrix} |E_{H0}|e^{i\phi_H} \\ |E_{V0}|e^{i\phi_V} \end{pmatrix} \tag{5}$$

where ϕ_i are the phases of the polarized states. This expression is called a *Jones vector* $\vec{J}$.

Moreover, the 2×2 scattering matrix expressed by (1) is a mapping of an incident Jones vector such that

$$S : \vec{J}_i \to \vec{J}_r, \quad \vec{J}_r = S\vec{J}_i \tag{6}$$

where $\vec{J}_i$ is an incident Jones vector and $\vec{J}_r$ is a reflected Jones vector. More importantly, the incident Jones vector is a free variable that one can manipulate. In matrix form, (6) can be rewritten as

$$\begin{pmatrix} E^r_{H0} \\ E^r_{V0} \end{pmatrix} = \begin{pmatrix} s_{HH} & s_{HV} \\ s_{VH} & s_{VV} \end{pmatrix} \begin{pmatrix} E^i_{H0} \\ E^i_{V0} \end{pmatrix}. \tag{7}$$

The coherency matrix (intensity) of the reflected Jones vector $\vec{J}_r$ is defined by

$$J = \begin{pmatrix} \langle E^r_{H0}E^{r*}_{H0}\rangle & \langle E^r_{H0}E^{r*}_{V0}\rangle \\ \langle E^r_{V0}E^{r*}_{H0}\rangle & \langle E^r_{V0}E^{r*}_{V0}\rangle \end{pmatrix} = \begin{pmatrix} J_{HH} & J_{HV} \\ J_{VH} & J_{VV} \end{pmatrix} \tag{8}$$

where $\langle\cdot\rangle$ stands for spatial averaging and * for conjugation. This expression is called a Jones coherency matrix of a reflected Jones vector. Furthermore, we reexpress this coherency matrix by

$$\begin{pmatrix} q_0 \\ q_1 \\ q_2 \\ q_3 \end{pmatrix} = \begin{pmatrix} |E_{H0}|^2 + |E_{V0}|^2 \\ |E_{H0}|^2 - |E_{V0}|^2 \\ 2|E_{H0}||E_{V0}|\cos\phi_{HV} \\ 2|E_{H0}||E_{V0}|\sin\phi_{HV} \end{pmatrix} = \begin{pmatrix} J_{HH} + J_{VV} \\ J_{HH} - J_{VV} \\ J_{VH} + J_{HV} \\ i(J_{HV} - J_{VH}) \end{pmatrix} \tag{9}$$

where q_1, q_2, and q_3 are *Stokes vectors*; $\phi_{HV} = \phi_H - \phi_V$ is the phase difference in radians with $\phi_H = arg(E_{H0})$, and $\phi_V = \arg(E_{V0})$. In addition, we normalize these *Stokes vectors* such that

$$q_1 = \frac{q_1}{q_0}, \quad q_2 = \frac{q_2}{q_0}, \quad q_3 = \frac{q_3}{q_0} \tag{10}$$

and the normalized q_1, q_2, and q_3 are called *Stokes parameters*.

III. Stokes Parameters of Our PolSAR Images

As real-world PolSAR images, we use the PolSAR images of *San Francisco* and *Oberpfaffenhofen* [see Fig. 4 (top)]. For any PolSAR image, its polarization-changing targets S can be represented by any numbers of Stokes parameters based on the incident Jones vector (a free variable).

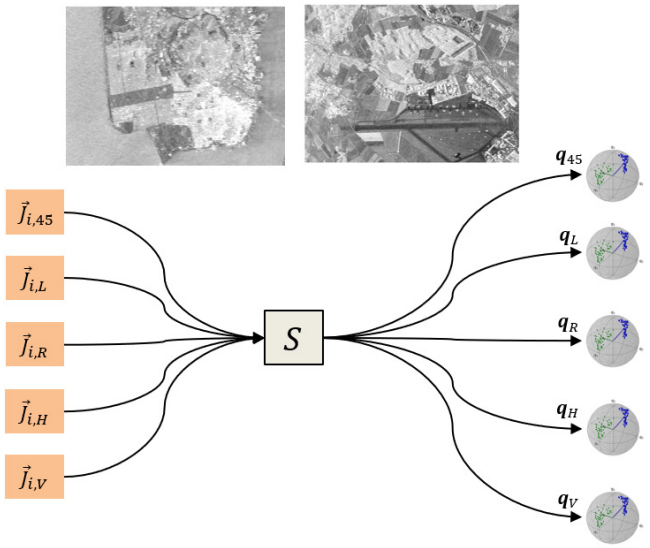

Fig. 4. Polarization-changing target S in a PolSAR image is represented by five Stokes parameters (features). (Top) PolSAR images of *San Francisco* and *Oberpfaffenhofen*. (Bottom; Left to Right) Incident Jones vectors, a polarization-changing target S, and the corresponding Stokes parameters.

In this article, we assume the incident Jones vector $\vec{J}_i \in \{\vec{J}_{i,45}, \vec{J}_{i,L}, \vec{J}_{i,R}, \vec{J}_{i,H}, \vec{J}_{i,V}\}$ shown in Fig. 4 (bottom)

$$\vec{J}_{i,45} = \frac{1}{\sqrt{2}}\begin{pmatrix} 1 \\ 1 \end{pmatrix}, \quad \vec{J}_{i,L} = \frac{1}{\sqrt{2}}\begin{pmatrix} 1 \\ i \end{pmatrix}, \quad \vec{J}_{i,R} = \frac{1}{\sqrt{2}}\begin{pmatrix} 1 \\ -i \end{pmatrix}$$
$$\vec{J}_{i,V} = \frac{1}{\sqrt{2}}\begin{pmatrix} 0 \\ 1 \end{pmatrix}, \quad \vec{J}_{i,H} = \frac{1}{\sqrt{2}}\begin{pmatrix} 1 \\ 0 \end{pmatrix} \tag{11}$$

where $\vec{J}_{i,45}$ is the polarized state along a 45° diagonal, $\vec{J}_{i,L}$ is the polarized state of the left-handed circular beam, $\vec{J}_{i,R}$ is the polarized state of the right-handed circular beam, $\vec{J}_{i,V}$ is the vertically polarized state, and $\vec{J}_{i,H}$ is the horizontally polarized state [21].

Then, we obtain each target of our PolSAR images the corresponding Stokes parameters by using (8)–(10)

$$\mathbf{q} = \{\mathbf{q}_{45}, \mathbf{q}_L, \mathbf{q}_R, \mathbf{q}_V, \mathbf{q}_H\}, \quad \mathbf{q}_i \in \mathbb{R}^3. \tag{12}$$

We characterize each target pixel by five Stokes parameters (features) by manipulating the incident Jones vector. More importantly, we have five times more features for each polarization-changing target in a PolSAR image than in an original image (see Fig. 4). We use these Stokes parameters as inputs of a hybrid quantum-classical network, as shown in step I of Fig. 5.

In Sections IV and V, we design a hybrid quantum-classical network, and we demonstrate how a hybrid quantum-classical network is programmed (using optimization and backpropagation) to update its weights when applying a synthetic quantum dataset as its input. For PolSAR images, we embed the Stokes parameters in the qubits of a hybrid quantum-classical network, as shown in step II of Fig. 5. Finally, we demonstrate the effectiveness of using PolSAR images in a hybrid quantum-classical network by recognizing the target classes of PolSAR images, namely, *San Francisco* and *Oberpfaffenhofen* (see step III of Fig. 5).

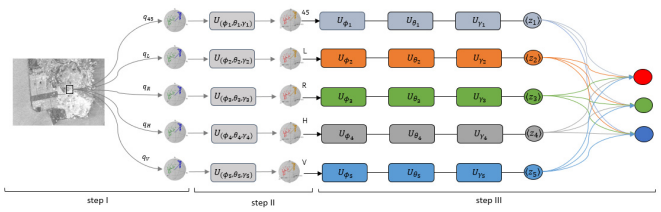

Fig. 5. General steps for a hybrid quantum-classical network for our PolSAR image, e.g., *San Francisco*: (step-I) Stokes parameters as inputs. (step-II) embedding of Stokes parameters in qubits. (step-III) hybrid quantum-classical network for analyzing PolSAR images.

IV. Hybrid Quantum-Classical Network

A QML network consists of *two-state qubits* and *parameterized quantum gates*. A *two-state qubit* is a complex vector in a Hilbert space denoted as a ket vector $|\psi\rangle \in \{|0\rangle, |1\rangle\}$

$$|0\rangle = \begin{pmatrix} 1 \\ 0 \end{pmatrix}, \quad |1\rangle = \begin{pmatrix} 0 \\ 1 \end{pmatrix} \tag{13}$$

and as a bra vector $\langle\psi| = |\psi\rangle^\dagger$, where † represents both transpose and conjugation. The two-state qubits can result in superposition as

$$|\psi\rangle = c_1|0\rangle + c_2|1\rangle \quad \text{s.t. } |c_1|^2 + |c_2|^2 = 1 \tag{14}$$

where c_1 and c_2 are complex numbers, and $P_i = |c_i|^2$ represents the probability for obtaining a state $|i\rangle$ after a measurement (see Fig. 6). Namely, in quantum physics, by measurements, we obtain the eigenvalue of an observable $\hat{z}$ with a certain probability P_i.

Parameterized quantum gates are unitary operators defined by

$$\hat{U} = \hat{U}(\gamma, \theta, \phi) = \hat{U}_\gamma \hat{U}_\theta \hat{U}_\phi \tag{15}$$

where γ, θ, and ϕ are parameters (angles), and they can be written in matrix form as

$$\hat{U}_\gamma = \begin{pmatrix} e^{i\gamma} & 0 \\ 0 & e^{-i\gamma} \end{pmatrix}, \quad \hat{U}_\theta = \begin{pmatrix} \cos(\theta) & -\sin(\theta) \\ \sin(\theta) & \cos(\theta) \end{pmatrix} \tag{16}$$

$$\hat{U}_\phi = \begin{pmatrix} e^{i\phi} & 0 \\ 0 & e^{-i\phi} \end{pmatrix}. \tag{17}$$

These unitary operators induce rotations of the qubits on/in the Bloch sphere [21] such that $|\psi'\rangle = \hat{U}|\psi\rangle$, as shown in Fig. 6.

For a QML network, we measure the expectation value of an operator $\hat{z}$, and the operator $\hat{z}$ is decomposed into its eigenvalues z_i and eigenvectors $|z_i\rangle$ as follows:

$$\hat{z} = \sum_i z_i |z_i\rangle\langle z_i|, \quad z_i \in \{-1, +1\}. \tag{18}$$

Then, the expectation value of an operator $\hat{z}$ is defined by

$$\langle z\rangle = \langle\psi|\hat{z}|\psi\rangle = \sum_i P_i z_i, \quad \langle z\rangle \in [-1, +1] \tag{19}$$

where P_i is the probability of obtaining the eigenvalue z_i given a quantum state $|\psi\rangle$.

Furthermore, we added a conventional layer of neurons to the outputs of a QML network. Such a network is called a

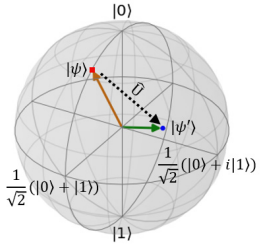

Fig. 6. Unitary transformation of a qubit into another qubit in/on the Bloch sphere. $\hat{U}:|\psi\rangle \rightarrow |\psi'\rangle$, where $|\psi\rangle = c_1|0\rangle + c_2|1\rangle$ and $\hat{U}|\psi\rangle = |\psi'\rangle = c_1'|0\rangle + c_2'|1\rangle$.

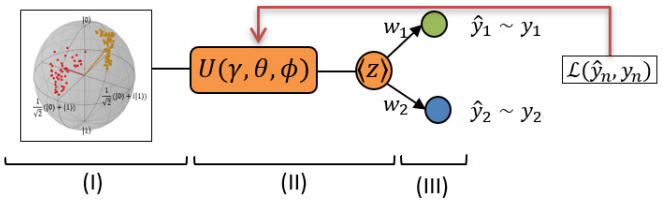

Fig. 7. Hybrid quantum-classical network for the classification of a quantum dataset: (I) Quantum dataset (qubits $|\psi\rangle$), (II) QML network, and (III) conventional layer of neurons, e.g., two neurons.

hybrid quantum-classical network, as shown in Fig. 7. For simplicity, we designed a hybrid quantum-classical network by using only three *parameterized quantum gates* expressed in (15) and a layer of two neurons for a binary quantum dataset. We used these unitary operators both for the embedding of classical data in qubits and for designing a hybrid quantum-classical network.

For programming the hybrid quantum-classical network, we expressed our expectation value by

$$\langle z\rangle = \langle\psi|U^\dagger(\gamma, \theta, \phi)\hat{z}U(\gamma, \theta, \phi)|\psi\rangle. \tag{20}$$

In addition, we assumed the above expectation value as a function

$$z(\theta_1, \theta_2, \theta_3) = \langle z\rangle \tag{21}$$

where $\theta_1 = \gamma, \theta_2 = \theta, \theta_3 = \phi$, and the outputs of the neurons are then expressed such that

$$\hat{y}_n = A(b_n + w_n z(\theta_1, \theta_2, \theta_3)) \tag{22}$$

where $A = A(\cdot)$ is a nonlinear activation function, $\hat{y}_n$ is its predicted output, b_n is its bias, and w_n is its edge parameter.

1) Optimization and Backpropagation: We have five parameters $\vec{w} = (w_1, w_2, \theta_1, \theta_2, \theta_3)$, and we optimize a total loss function $\mathcal{L} = \mathcal{L}(\hat{y}_n, y_n)$; namely, we update and learn the parameters as follows:

$$\vec{w}_{\text{new}} = \vec{w}_{\text{old}} - \lambda \nabla \cdot \mathcal{L} \tag{23}$$

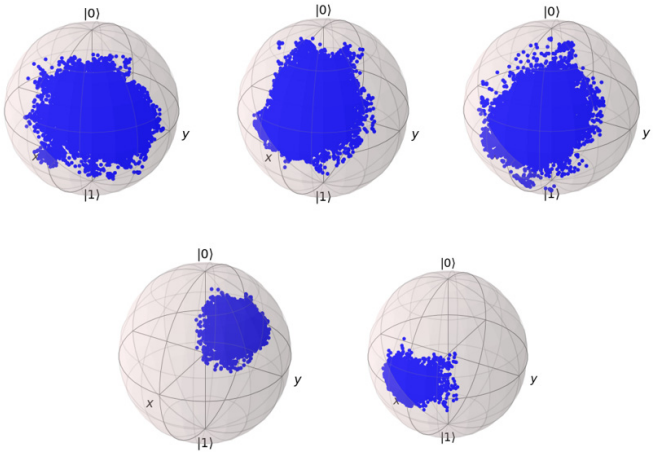

Fig. 8. For *San Francisco*, its embedded Stokes parameters in qubits. Each Stokes parameter carries different information of a polarization-changing target. (Top Left) Qubits with $\mathbf{q}_{45}$. (Top Middle) Qubits with $\mathbf{q}_L$. (Top Right) Qubits with $\mathbf{q}_R$. (Bottom Left) Qubits with $\mathbf{q}_V$. (Bottom Right) Qubits with $\mathbf{q}_H$.

where λ is the learning rate, and by backpropagation, we obtain

$$\begin{aligned}
\nabla \cdot \mathcal{L} &= (\partial\mathcal{L}/\partial w_1, \partial\mathcal{L}/\partial w_2, \partial\mathcal{L}/\partial\theta_1, \partial\mathcal{L}/\theta_2, \partial\mathcal{L}/\partial\theta_3)^{\mathrm{T}} \\
\frac{\partial\mathcal{L}}{\partial w_n} &= \frac{\partial\mathcal{L}}{\partial\hat{y}_n}\frac{\partial\hat{y}_n}{\partial w_n}, \quad n = 1, 2 \\
\frac{\partial\mathcal{L}}{\partial\theta_i} &= \sum_{n=1}^{2} \frac{\partial\mathcal{L}}{\partial\hat{y}_n}\frac{\partial\hat{y}_n}{\partial z(\theta_1,\theta_2,\theta_3)}\frac{\partial z(\theta_1,\theta_2,\theta_3)}{\partial\theta_i}, \quad i = 1, 2, 3
\end{aligned} \tag{24}$$

which we compute on a conventional computer.

V. Processing of a Synthetic Quantum Dataset on a Hybrid Quantum-Classical Network

As a proof of concept, we analyzed a small set of a synthetic quantum dataset, and we used the hybrid quantum-classical network shown in Fig. 7. It has the advantage that we could easily understand the implementation and the performance of a hybrid quantum-classical network.

In our case, the synthetic quantum dataset consists of the points $(|\psi\rangle_n, y_n)$, $n = 1, 2, \ldots, 100$, where its first half corresponds to a class $y_n = (1, 0)$ represented in yellow in Fig. 7, and its other half corresponds to a class $y_n = (0, 1)$ represented in red in Fig. 7. We generated this quantum dataset according to

$$|\psi\rangle_n = \cos\left(\frac{\alpha}{2}\right)|0\rangle_n + e^{i\beta}\sin\left(\frac{\alpha}{2}\right)|1\rangle_n \tag{25}$$

where we assumed $\alpha = 0.6$ for a class label $y_n = (0, 1)$ and $\alpha = 3$ for a class label $y_n = (1, 0)$. Hence, we did not need the embedding procedure.

For the implementation of the hybrid quantum-classical network, we employed an IBM quantum computer (an *ibmq-armonk* qubit) and a classical simulator for a quantum computer; here, the *ibmq-armonk* qubit of an IBM quantum computer is a noisy qubit, while the qubit of a classical simulator is a perfect one. With both of these quantum computers

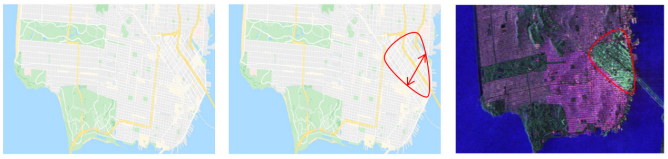

Fig. 9. Visualization of *San Francisco*. (Left) Google map of *San Francisco* exhibiting the classes *urban area*, *vegetation*, and *sea water*. (Middle) Red contour presents a part of the *urban area* with a different orientation (see the red arrow); namely, a *rotated urban area*. (Right) Visualization of the Pauli vectors of *San Francisco* expressed by (2). The Pauli vector clearly distinguishes the *rotated urban area* from the remainder of the *urban area*. Blue: *sea water* (a single-bounced beam). Pink: *urban area* (a double-bounced beam). Light green: *rotated urban area* (inside the red contour) with a different orientation from the remainder (a volume-scattered beam). Dark green: *vegetation* (a volume-scattered beam).

and a classical simulator, we reached a classification *accuracy* and *loss* of $(1.000, 0.0083)$ for our synthetic quantum dataset. This finding leads to the very important conclusion that for a noisy quantum computer, our hybrid network does not need any error correction processing for a noisy qubit. More importantly, the classical layer of our hybrid network corrects a classification mistake made by a noisy qubit.

The insights gained from the classification of our synthetic quantum dataset on the hybrid quantum-classical network are given as follows.

1) A classical dataset needs to be *naturally* embedded in qubits due to the very small number of qubits.
2) A hybrid quantum-classical network does not need any error correction processing for a noisy qubit. This could be proven by the accuracy of our experiment on a synthetic quantum dataset.
3) A classical layer handles the mistakes made by a noisy qubit.
4) The publicly available IBM quantum computer has a very high overhead.

VI. Embedding and Processing of PolSAR Images in a Hybrid Quantum-Classical Network

A. Embedding the Stokes Parameters of PolSAR Images in Qubits

We used the PolSAR images of *San Francisco* and *Oberpfaffenhofen* for processing in a hybrid quantum-classical network, and we represented them by the Stokes parameters $\mathbf{q} = (\mathbf{q}_{45}, \mathbf{q}_L, \mathbf{q}_R, \mathbf{q}_V, \mathbf{q}_H)$ presented in Section III. Here, we embedded the Stokes parameters in the qubits of a hybrid quantum-classical network by applying (15). The Stokes parameters of *San Francisco* and *Oberpfaffenhofen* are naturally equivalent to qubits due to the Doppelganger role of reflected Jones vectors and qubits. The advantage is that we do not need to reduce our PolSAR images in their given spatial dimensionality or train another QML network to embed them in qubits. Thus, we embedded the Stokes parameters in qubits in a two-step procedure.

1) A single-qubit is prepared in a state $|0\rangle$.
2) The Stokes parameters $\mathbf{q}_i$ for each pixel of our PolSAR images are embedded in qubits by using (15) such that

$$U(\gamma_1, \theta_2, \phi_3) : |0\rangle \rightarrow |\psi\rangle, \quad |\psi\rangle = U(\gamma_1, \theta_2, \phi_3)|0\rangle$$

where $\gamma_1 = q_1$, $\theta_2 = q_2$, and $\phi_3 = q_3$ are elements of each $\mathbf{q}_i, i = 45, L, R, V, H$; the state $|\psi\rangle$ sits in/on a Bloch sphere.

For the case of the PolSAR image of *San Francisco*, we show its embedded Stokes parameters carrying different scattering properties for targets in Fig. 8.

B. Processing PolSAR Images in a Hybrid Quantum-Classical Network

We processed the PolSAR images *San Francisco* and *Oberpfaffenhofen* by exploiting their five Stokes parameters in a hybrid quantum-classical network. In particular, we analyzed that whether the Stokes parameters of a given PolSAR image carry some physical scattering properties of polarization-changing targets by recognizing them in a hybrid quantum-classical network. The physical scattering properties are a *single-bounced beam*, a *double-bounced beam*, and a *volume-scattered beam* on polarization-changing targets (see Figs. 3 and 9). Here, we use the PolSAR image of *San Francisco* as a training and a validation dataset and the PolSAR image of *Oberpfaffenhofen* as a test dataset.

For the training dataset, we selected four classes of *San Francisco* that are *urban area* (its physical scattering property: a double-bounced beam), *rotated urban area* (its physical scattering property: a volume-scattered beam), *sea water* (its physical scattering property: a single-bounced beam), and *vegetation* (its physical scattering property: a volume-scattered beam) shown in Fig. 9 [22], [23]; each class image has a size of 590 × 497 pixels. Once having defined our training dataset, we designed our experiment by the following procedures (see step-I and step-III in Fig. 5).

1) Derive the five Stokes parameters from our training dataset.
2) Embed these Stokes parameters in qubits by Steps 1) and 2) of Section VI-A.
3) Design/train a hybrid quantum-classical network.
4) Employ an *Adam* optimizer and the categorical cross entropy for the training process.

Then, we ran our experiment for the recognition of targets in *San Francisco* in three different scenarios.

A first scenario for the binary classes urban area and *rotated urban area is* given as follows.

1) We represented these binary classes only by the Stokes parameter $\mathbf{q}_{45}$.
2) We embedded $\mathbf{q}_{45}$ in qubits and trained the qubits by employing the hybrid quantum-classical network shown in Fig. 10.
3) The validation accuracy reached 0.8005.

In this first scenario, we represented the binary classes of *urban area* and *rotated urban area* of *San Francisco* by the Stokes parameter $\mathbf{q}_{45}$. Then, we trained and distinguished them by applying the hybrid quantum-classical network shown in Fig. 10. Finally, we compared our detected results with respect to their Pauli vectors (see Fig. 11). This comparison confirms that the Stokes parameter $\mathbf{q}_{45}$ describes the physical scattering properties of *urban area* and *rotated urban area*.

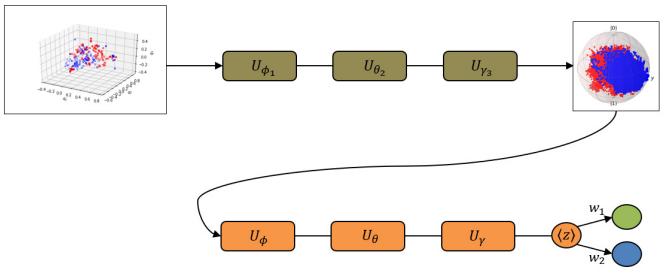

Fig. 10. Our hybrid quantum-classical network for the embedding and the training of our binary classes of *San Francisco* with $\mathbf{q}_{45}$. (Top) Embedding of our Stokes parameter $\mathbf{q}_{45}$ in qubits. (Bottom) hybrid quantum-classical network for training these qubits.

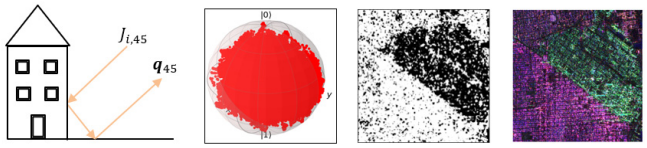

Fig. 11. (Left to Right) *urban area* and the *rotated urban area* of *San Francisco* are characterized by the Stokes parameter $\mathbf{q}_{45}$, the embedded Stokes parameters in qubits, the visual results for the binary classification (*urban area* and *rotated urban area*) in our hybrid quantum-classical network shown in Fig. 10, and the Pauli vector of *urban area* and *rotated urban area*.

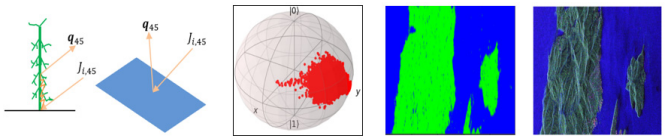

Fig. 12. (Left to Right) *Sea water* and *vegetation* of *San Francisco* are characterized by the Stokes parameter $\mathbf{q}_{45}$, the embedded Stokes parameters in qubits, the visual results for the binary classification (*sea water* and *vegetation*) in our hybrid quantum-classical network shown in Fig. 10, and the Pauli vector of *sea water* and *vegetation*.

A second scenario for the binary class sea water and *vegetation is* given as follows.

1) We represented this binary class only by the Stokes parameter $\mathbf{q}_{45}$.
2) We embedded $\mathbf{q}_{45}$ in qubits and trained the qubits by employing the hybrid quantum-classical network shown in Fig. 10.
3) The validation accuracy reached 0.9613.

In this second scenario, we represented the binary class of *sea water* and *vegetation* by the Stokes parameter $\mathbf{q}_{45}$. Then, we trained and recognized the classes by applying the hybrid quantum-classical network shown in Fig. 10 as in the previous scenario. We also benchmarked our findings with respect to their Pauli vectors; the visual (target recognition) result and their Pauli vector are shown in Fig. 12. This visual result again proves that the Stokes parameter $\mathbf{q}_{45}$ characterizes the physical scattering properties of *sea water* and *vegetation*.

A final scenario for the three classes, *vegetation*, *urban area*, and *sea water*, *is* given as follows.

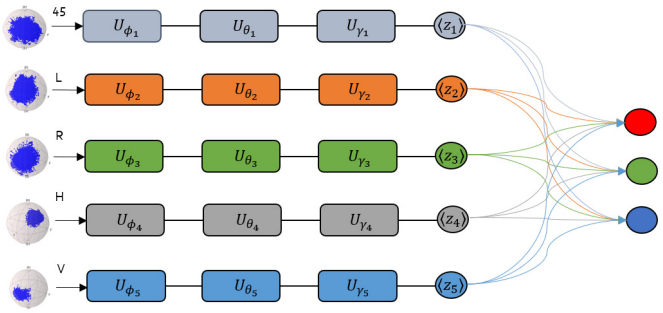

Fig. 13. Hybrid quantum-classical network for the training of three classes of *San Francisco* with five simultaneous inputs of $\mathbf{q}_i$. The hybrid quantum-classical network for the training of given qubits (the embedding of Stokes parameters in qubits is not shown).

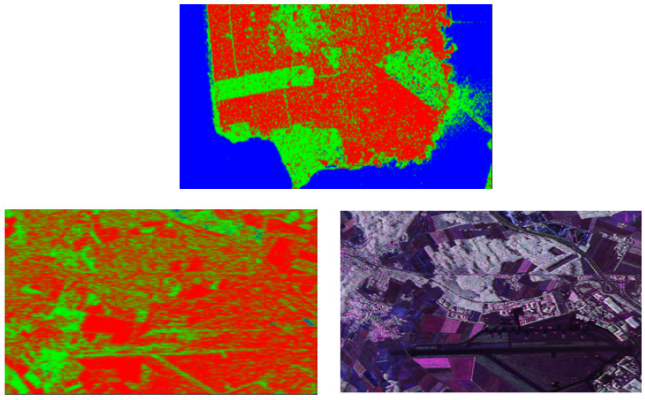

Fig. 14. Recognition of targets in PolSAR images (*blue*: a single-bounced beam, *red*: a double-bounced beam, and *green*: a volume-scattered beam). (Top) Target recognition in the PolSAR image of *San Francisco*. (Bottom Left) Targets recognition in the PolSAR image of *Oberpfaffenhofen*. (Right) Pauli vector of the PolSAR image of *Oberpfaffenhofen*.

1) We represented these three classes by the Stokes parameters $\mathbf{q} = (\mathbf{q}_{45}, \mathbf{q}_L, \mathbf{q}_R, \mathbf{q}_V, \mathbf{q}_H)$.
2) We embedded $\mathbf{q}$ in qubits and trained the three classes by applying the hybrid quantum-classical network shown in Fig. 13.
3) The validation accuracy reached 0.8362.

In this final scenario, we represented each target of our PolSAR image by five Stokes parameters $\mathbf{q} = (\mathbf{q}_{45}, \mathbf{q}_L, \mathbf{q}_R, \mathbf{q}_V, \mathbf{q}_H)$, and we trained them by using the hybrid quantum-classical network shown in Fig. 13. We visualize the identified results in Fig. 14 Top. The visual results demonstrate that our network identified *vegetation* and *rotated urban area* as the same class due do the same physical scattering property, namely, a volume-scattered beam [see Fig. 9 (right)]. This result conclusively proves that the Stokes parameters contain the physical scattering properties of targets.

Furthermore, we even tested our trained hybrid quantum-classical network on *Oberpfaffenhofen* and verified our test result with respect to its Pauli vector. The visual results explicitly show that our network recognized the physical scattering properties of targets in the PolSAR image of *Oberpfaffenhofen* [see Fig. 14 (bottom)].

VII. Conclusion

The inputs of quantum algorithms are quantum data, and for practical applications, there is a persisting challenge to map classical data to quantum data. Hence, we provided real-world EO measurement data that inherit quantum nature; in particular, PolSAR images. The PolSAR images consist of polarization-changing targets that are characterized by the reflected Jones vectors. The reflected Jones vectors are the Doppelganger of qubits. Therefore, we mapped the reflected Jones vectors (the Stokes parameters) of PolSAR images to quantum bits, and we designed and provided hybrid quantum-classical networks as a quantum algorithm to prove that we *naturally* embedded our data in qubits. Then, we investigated whether the Stokes parameters convey the physical scattering properties of the targets of PolSAR images by recognizing them in our hybrid quantum-classical networks. In this work, we represented the targets of PolSAR images by five Stokes parameters. As real-world PolSAR images, we used two types of PolSAR images, namely, *San Francisco* and *Oberpfaffenhofen*.

In more detail, we provided PolSAR images with a *natural embedding* feature and investigated whether their Stokes parameters convey the physical scattering properties of the PolSAR images by recognizing them in the hybrid quantum-classical networks. We processed the PolSAR image of *San Francisco* in three different scenarios of its Stokes parameters by using two different hybrid quantum-classical networks. After training these hybrid quantum-classical networks in different scenarios for the Stokes parameters of *San Francisco*, we tested these trained hybrid quantum-classical networks on the PolSAR image of *Oberpfaffenhofen*. Our obtained results demonstrate that the Stokes parameters convey the physical scattering properties of PolSAR images. In addition, we ran our hybrid quantum-classical network both on an IBM quantum computer and a classical simulator of a quantum computer. The classical layer of our hybrid quantum-classical network corrects an error made by a noisy qubit (*ibmq-armonk*) of the IBM quantum computer; the IBM quantum computer that is publicly available has a high overhead.

In terms of our ongoing and future work, we study deeply a hybrid quantum-classical network and future quantum computing platforms for processing PolSAR images due to the Doppelganger role of the Jones vectors and qubits. Furthermore, we design a hybrid quantum-classical network for distinguishing targets with the same physical scattering properties in PolSAR images.

Acknowledgment

The authors would like to greatly acknowledge Gottfried Schwarz (DLR, Oberpfaffenhofen) for his valuable comments and contributions for enhancing the quality of this article.

References

[1] J. Preskill, "Quantum computing in the NISQ era and beyond," *Quantum*, vol. 2, p. 79, Aug. 2018, doi: 10.22331/q-2018-08-06-79.

[2] S. Otgonbaatar and M. Datcu, "A quantum annealer for subset feature selection and the classification of hyperspectral images," *IEEE J. Sel. Topics Appl. Earth Observ. Remote Sens.*, vol. 14, pp. 7057–7065, Jul. 2021. [Online]. Available: https://ieeexplore.ieee.org/document/9477115/
[3] J. Biamonte, P. Wittek, N. Pancotti, P. Rebentrost, N. Wiebe, and S. Lloyd, "Quantum machine learning," *Nature*, vol. 549, no. 7671, pp. 195–202, Sep. 2017, doi: 10.1038/nature23474.
[4] V. Dunjko and H. J. Briegel, "Machine learning & artificial intelligence in the quantum domain: A review of recent progress," *Rep. Prog. Phys.*, vol. 81, no. 7, Jun. 2018, Art. no. 074001, doi: 10.1088/1361-6633/aab406.
[5] P. Rebentrost, M. Mohseni, and S. Lloyd, "Quantum support vector machine for big data classification," *Phys. Rev. Lett.*, vol. 113, Sep. 2014, Art. no. 130503, doi: 10.1103/PhysRevLett.113.130503.
[6] S. Lloyd, M. Mohseni, and P. Rebentrost, "Quantum principal component analysis," *Nature Phys.*, vol. 10, pp. 631–633, Jul. 2014, doi: 10.1038/nphys3029.
[7] N. H. Nguyen, E. C. Behrman, M. A. Moustafa, and J. E. Steck, "Benchmarking neural networks for quantum computations," *IEEE Trans. Neural Netw. Learn. Syst.*, vol. 31, no. 7, pp. 2522–2531, Jul. 2020.
[8] Y. Li, M. Tian, G. Liu, C. Peng, and L. Jiao, "Quantum optimization and quantum learning: A survey," *IEEE Access*, vol. 8, pp. 23568–23593, Jan. 2020.
[9] H.-Y. Huang *et al.*, "Power of data in quantum machine learning," *Nature Commun.*, vol. 12, no. 1, pp. 1–9, May 2021, doi: 10.1038/s41467-021-22539-9.
[10] J. M. Kübler, S. Buchholz, and B. Schölkopf, "The inductive bias of quantum kernels," 2021, *arXiv:2106.03747*. [Online]. Available: http://arxiv.org/abs/2106.03747
[11] M. Schuld and N. Killoran, "Quantum machine learning in feature Hilbert spaces," *Phys. Rev. Lett.*, vol. 122, Feb. 2019, Art. no. 040504, doi: 10.1103/PhysRevLett.122.040504.
[12] S. Lloyd, M. Schuld, A. Ijaz, J. Izaac, and N. Killoran, "Quantum embeddings for machine learning," May 2020, *arXiv:2001.03622*. [Online]. Available: http://arxiv.org/abs/2001.03622
[13] S. R. Cloude and K. P. Papathanassiou, "Polarimetric SAR interferometry," *IEEE Trans. Geosci. Remote Sens.*, vol. 36, no. 5, pp. 1551–1565, Sep. 1998.
[14] S. R. Cloude and E. Pottier, "An entropy based classification scheme for land applications of polarimetric SAR," *IEEE Trans. Geosci. Remote Sens.*, vol. 35, no. 1, pp. 68–78, Jan. 1997.
[15] A. G. Mullissa, C. Persello, and A. Stein, "PolSARNet: A deep fully convolutional network for polarimetric SAR image classification," *IEEE J. Sel. Topics Appl. Earth Observ. Remote Sens.*, vol. 12, no. 12, pp. 5300–5309, Dec. 2019.
[16] J. S. Lee *et al.*, "A review of polarimetric SAR algorithms and their applications," *J. Photogram. Remote Sens.*, vol. 9, no. 3, pp. 31–80, 2004.
[17] A. Moreira, P. Prats-Iraola, M. Younis, G. Krieger, I. Hajnsek, and K. P. Papathanassiou, "A tutorial on synthetic aperture radar," *IEEE Geosci. Remote Sens. Mag.*, vol. 1, no. 1, pp. 6–43, Mar. 2013.
[18] H. Dong, B. Zou, L. Zhang, and S. Zhang, "Automatic design of CNNs via differentiable neural architecture search for PolSAR image classification," *IEEE Trans. Geosci. Remote Sens.*, vol. 58, no. 9, pp. 6362–6375, Sep. 2020.
[19] F. Shang and A. Hirose, "Quaternion neural-network-based PolSAR land classification in Poincare-sphere-parameter space," *IEEE Trans. Geosci. Remote Sens.*, vol. 52, no. 9, pp. 5693–5703, Sep. 2014.
[20] G. Singh, S. Mohanty, Y. Yamazaki, and Y. Yamaguchi, "Physical scattering interpretation of POLSAR coherency matrix by using compound scattering phenomenon," *IEEE Trans. Geosci. Remote Sens.*, vol. 58, no. 4, pp. 2541–2556, Apr. 2020.
[21] S. Barnett, Ed., *Quantum Information*. London, U.K.: Oxford Univ. Press, 2009.
[22] D. Ratha, A. Bhattacharya, and A. C. Frery, "Unsupervised classification of PolSAR data using a scattering similarity measure derived from a geodesic distance," *IEEE Geosci. Remote Sens. Lett.*, vol. 15, no. 1, pp. 151–155, Jan. 2018.
[23] S. Dey, A. Bhattacharya, D. Ratha, D. Mandal, and A. C. Frery, "Target characterization and scattering power decomposition for full and compact polarimetric SAR data," *IEEE Trans. Geosci. Remote Sens.*, vol. 59, no. 5, pp. 3981–3998, May 2021.

Soronzonbold Otgonbaatar received the B.Sc. degree from the National University of Mongolia, Ulaanbaatar, Mongolia, in 2014, and the M.Sc. degree in theoretical particle physics from the University of Siegen, Siegen, Germany, in 2016. He is currently pursuing the Ph.D. degree with German Aerospace Center, Weßling, Germany.

His research interests include computational science, artificial intelligence (i.e., machine learning), quantum computing and algorithms, and quantum machine learning with practical applications in remote sensing data.

Mihai Datcu (Fellow, IEEE) received the M.S. and Ph.D. degrees in electronics and telecommunications from the University Politehnica of Bucharest (UPB), Bucharest, Romania, in 1978 and 1986, respectively, and the Habilitation a Diriger Des Recherches degree in computer science from Louis Pasteur University, Strasbourg, France, in 1999.

From 1992 to 2002, he had a longer Invited Professor Assignment with the Swiss Federal Institute of Technology (ETH Zürich), Zürich, Switzerland. He was a Visiting Professor with the University of Oviedo, Oviedo, Spain; Louis Pasteur University; International Space University, Strasbourg; the University of Siegen, Siegen, Germany; the University of Innsbruck, Innsbruck, Austria; the University of Alcalá, Alcalá de Henares, Spain; Tor Vergata University, Rome, Italy; the Universidad Pontificia de Salamanca, Madrid, Spain; the University of Camerino, Camerino, Italy; and the Swiss Center for Scientific Computing, Manno, Switzerland. Since 1981, he has been a Professor with the Department of Applied Electronics and Information Engineering, Faculty of Electronics, Telecommunications and Information Technology, UPB. Since 1993, he has been a Scientist with the German Aerospace Center (DLR), Weßling, Germany. He is developing algorithms for model-based information retrieval from high-complexity signals and methods for scene understanding from very-high-resolution synthetic aperture radar (SAR) and interferometric SAR data. Since 2011, he has been leading the Immersive Visual Information Mining Research Laboratory, Munich Aerospace Faculty, and he is the Director of the Research Center for Spatial Information, UPB. Since 2001, he has been initiating and leading the Competence Center on Information Extraction and Image Understanding for Earth Observation, ParisTech, Paris Institute of Technology, Télécom Paris, Paris, France, a collaboration of DLR with the French Space Agency (CNES). He has been a Professor with the DLR-CNES Chair, ParisTech, Paris Institute of Technology, Télécom Paris. He has initiated the European frame of projects for image information mining (IIM) and is involved in research programs for information extraction, data mining and knowledge discovery, and data understanding with the European Space Agency (ESA), Paris, NASA, and in a variety of national and European projects. He and his team have developed and are developing the operational IIM processor in the Payload Ground Segment systems for the German missions, TerraSAR-X, TanDEM-X, and the ESA Sentinel-1 and Sentinel-2. He is currently a Senior Scientist and the Data Intelligence and Knowledge Discovery Research Group Leader with the Remote Sensing Technology Institute, DLR, and involved in the DLR-ONERA Joint Virtual Center for AI in Aerospace. He is also a Visiting Professor with the ESA's Φ-Lab. His research interests include explainable and physics-aware artificial intelligence, smart sensors design, and quantum machine learning with applications in earth observation.

Dr. Datcu is also a member of the ESA Working Group Big Data from Space. He was a recipient of the Best Paper Award and the IEEE Geoscience and Remote Sensing Society Prize in 2006, the National Order of Merit with the Rank of Knight, for outstanding international research results, awarded by the President of Romania, in 2008, and the Romanian Academy Prize Traian Vuia for the development of the SAADI image analysis system and his activity in image processing in 1987. He was also a recipient of the Chaire d'excellence internationale Blaise Pascal 2017 for international recognition in the field of data science in earth observation. He has served as a Co-Organizer for international conferences and workshops and a Guest Editor for special issues on AI, quantum machine learning, or big data of the IEEE and other journals.